



Published in final edited form as:

Nat Metab. 2022 April ; 4(4): 435–443. doi:10.1038/s42255-022-00553-5.

Altered propionate metabolism contributes to tumor progression and aggressiveness

Ana P. Gomes^{1,2,8,*,#}, **Didem Ilter**^{1,2,8,*}, **Vivien Low**^{1,2,*}, **Stanislav Drapela**³, **Tanya Schild**^{1,2,10}, **Edouard Mullarky**^{1,4}, **Julie Han**^{1,2}, **Ilaria Elia**^{5,6}, **Dorien Broekaert**^{5,6}, **Adam Rosenzweig**^{1,2}, **Michal Nagiec**^{1,2}, **Joana B. Nunes**^{1,2}, **Bethany E. Schaffer**^{1,2}, **Anders P. Mutvei**^{1,2,9}, **John M. Asara**⁷, **Lewis C. Cantley**^{1,4}, **Sarah-Maria Fendt**^{5,6}, **John Blenis**^{1,2,#}

¹Meyer Cancer Center, Weill Cornell Medicine, New York, NY, USA.

²Department of Pharmacology, Weill Cornell Medicine, New York, NY, USA.

³Department of Molecular Oncology, H. Lee Moffit Cancer Center & Research Institute, Tampa, FL, USA.

⁴Department of Medicine, Weill Cornell Medicine, New York, NY, USA.

⁵Laboratory of Cellular Metabolism and Metabolic Regulation, VIB Center for Cancer Biology, VIB, Leuven, Belgium

⁶Laboratory of Cellular Metabolism and Metabolic Regulation, Department of Oncology, KU Leuven and Leuven Cancer Institute (LKI), Leuven, Belgium

⁷Department of Medicine, Beth Israel Deaconess Medical Center and Harvard Medical School, Boston, MA, USA.

⁸Present address: Department of Molecular Oncology, H. Lee Moffit Cancer Center & Research Institute, Tampa, FL, USA.

⁹Present address: Department of Immunology, Genetics and Pathology, Uppsala University, Uppsala, Sweden

¹⁰Present address: Department of Radiology, Memorial Sloan Kettering Cancer Center, New York, NY, USA

Users may view, print, copy, and download text and data-mine the content in such documents, for the purposes of academic research, subject always to the full Conditions of use: <https://www.springernature.com/gp/open-research/policies/accepted-manuscript-terms>

Corresponding authors: ana.gomes@moffitt.org; job2064@med.cornell.edu.

*Equal Contribution

Author Contributions Statement

A.P.G and J.B. conceived the project. A.P.G. and D.I. performed all the molecular biology experiments, the EMT-related experiments, the invasion and migration experiments, prepared the RNA for RNA-seq experiments and assisted on all other experiments. V.L. and T.S. performed all the mouse experiments and assisted on all other experiments. S.D. assisted with the MCEE analysis in patient samples and performed the proliferation assays. A.P.M. and B.S. quantified the migration and invasion experiments. A.R. produced the viral particles, generated the genetically modified cell lines, performed the qPCR analysis of MCEE and assisted with metabolite extractions and MMA measurements. J.H. generated the constructs and assisted in the EMT-related experiments. D.B. and I.E. collected the tumor and metastases tissues and prepared the samples for metabolomic analysis. T.S. and E.M. prepared and analyzed the C13 tracing analysis and assisted on all other metabolite measurements. M.N. and J.N. optimized the ERK2-D319N mutant. J.A. performed the metabolomics analysis. A.P.G., J.A., L.C.C., S.M.F. and J.B. supervised the project. A.P.G., D.I., V.L., A.M., B.S., E.M. and J.B. analyzed the data. The manuscript was written by A.P.G., V.L. and J.B., and edited by D.I., T.S., I.E., B.S. and S.M.F. All authors discussed the results and approved the manuscript.

Abstract

The alteration of metabolic pathways is a critical strategy for cancer cells to attain the traits necessary for metastasis in disease progression. Here, we find that dysregulation of propionate metabolism produces a pro-aggressive signature in breast and lung cancer cells, increasing their metastatic potential. This occurs through the downregulation of methylmalonyl-CoA epimerase (MCEE), mediated by an ERK2-driven SP1/EGR1 transcriptional switch driven by metastatic signaling at its promoter level. The loss of MCEE results in reduced propionate-driven anaplerotic flux and the intracellular and intratumoral accumulation of methylmalonic acid (MMA), a byproduct of propionate metabolism that promotes cancer cell invasiveness. Altogether, we present a previously uncharacterized dysregulation of propionate metabolism as an important contributor to cancer and a valuable potential target in the therapeutic treatment of metastatic carcinomas.

Cancer is the second leading cause of death worldwide, and metastatic cancer accounts for the major proportion of these mortalities^{1,2}. The reprogramming of cellular metabolism for both the development of cancer and its progression to metastasis presents a ripe area of research. Far from simply existing as the process of breakdown and buildup of nutrients in the cell, cellular metabolism has become recognized as a fundamental determinant of cellular identity and function³. It is now evident that certain metabolites, known as oncometabolites, can drive cancer progression and metastasis, functioning in autocrine, paracrine and endocrine fashions⁴. While the influence of age, diet and lifestyle on metabolism and consequently cancer progression is well established, the study of metabolic alterations that occur on the level of the tumor microenvironment present exciting new avenues for targeted therapies. Recently, we demonstrated how a systemic age-induced increase of a metabolite, methylmalonic acid (MMA), contributes to poor cancer prognosis and increased cancer-related mortality in elderly patients⁵, highlighting the importance of metabolic alterations in determining tumor progression.

Cancers, especially highly aggressive cancers, are notorious for their ability to hijack physiological processes to enable their progression. To characterize the relevant metabolic changes that promote cancer progression, we identified significantly altered metabolites in pulmonary metastases compared to corresponding primary tumors in the 4T1 orthotopic mouse model⁶ for triple negative breast cancer (TNBC) and performed a pathway enrichment analysis on these metabolites (Supplementary Table 1, Fig. 1a–b). It is important to note that while this experiment can provide a snapshot of potential metabolites and metabolic pathways that are important for TNBC metastasis, it likely does not account for the full spectrum of metabolic alterations that fuel metastasis. Through this analysis, we identified processes previously known to be affected in cancer progression, such as serine metabolism and ammonia recycling^{7–9}. Intriguingly, we also found the propionate metabolism pathway enriched in metastatic tumors, of which methylmalonic acid (MMA), a systemically increased aging-induced metabolite that we recently identified to contribute to metastatic aggressiveness, is a byproduct⁵ (Fig. 1c). Based on these results, we hypothesized that TNBC cells may hijack propionate metabolism in order to accumulate MMA, abetting a metabolic change that enhances metastatic success. To test if increased MMA levels within the tumor was correlated with metastasis, we measured MMA concentrations using LC-MS/MS in the primary tumors against the metastatic tumors of a 4T1 breast tumor

mouse model. Indeed, MMA concentrations were significantly higher in metastases than in primary tumors (Fig. 1d). Additionally, among clonal subpopulations isolated from a single mammary tumor, MMA levels were significantly higher in a broadly metastatic 4T1 clone, which is able to form metastases, compared to a locally invasive 4T07 clone, which has the ability to invade out of the primary tumor but remains metastatically dormant and fails to colonize secondary niches (Fig. 1e)¹⁰. These observations raised the question of whether increased MMA production could be generalizable to human cancer, so we measured MMA levels in a panel of human breast cell lines, including one breast epithelial cell line, three receptor positive breast cancer cell lines and four TNBC metastatic-like cell lines (Fig. 1f, Extended Data Fig. 1e). We observed a marked increase in the metastatic TNBC cell lines compared to the receptor positive breast cancer or breast epithelial cell lines, suggesting a conserved increase in MMA production in human metastatic TNBCs (Fig. 1f, Extended Data Fig. 1e). Together, these observations suggest that the production of MMA may be important for successful metastasis of TNBCs.

In order to establish if the increase in intracellular MMA levels was an early and potentially driving event in the metastatic process, we treated MCF10A and HCC1806 cells, a receptor-negative breast epithelial and primary TNBC cell line, respectively, with the metastatic inducers TGF β and TNF α ¹¹. Inflammatory cytokines, particularly TGF β and TNF α , have long been known to contribute to acquisition of metastatic properties, particularly through their ability to induce EMT in cancer cells, as well as by their ability to promote a permissive tumor microenvironment¹². Three days of TGF β /TNF α treatment was sufficient to increase MMA levels in these cells, consistent with its ability to promote EMT and the acquisition of pro-aggressive traits (Fig. 2a, 2b, 2d). We then set out to determine if MMA was being produced from propionyl-CoA or from intermediates of the TCA cycle, using a combination of ¹³C-labeled valine, isoleucine, threonine and methionine (AA) to monitor flux through the propionate metabolism pathway, or ¹³C-labeled glucose and glutamine (GG) to measure their contribution to MMA production via the TCA cycle. Although we cannot exclude a substantial contribution of odd chain fatty acid (OCFA) catabolism, our data show that a major fraction of the increase in intracellular MMA was derived from catabolism of AA through the propionate metabolic pathway (Fig. 2c). To determine how MMA was being increased, we surveyed expression of the enzymes involved in propionate metabolism. In MCF-10A and HCC1806 cells, TGF β /TNF α promoted a loss of methylmalonyl-CoA epimerase (MCEE) expression that coincided with the loss of epithelial and gain of mesenchymal markers (Fig. 2d). MCEE converts the D-isomer of methylmalonyl-CoA to the L-isomer that can be acted upon downstream by methylmalonyl-CoA mutase (MUT) to produce succinyl-CoA, which subsequently feeds into the TCA cycle (Fig. 1c). MCEE loss results in accumulation of D-methylmalonyl CoA and consequently, increased MMA, as seen in TGF β /TNF α mediated repression of MCEE (Fig. 1c, 2a–b). Additionally, we found that MCEE loss correlated with the metastatic ability of 4T1 clones, with decreased expression in broadly metastatic compared to locally invasive clones (Extended Data Fig. 1a). We also observed decreased protein expression of MCEE in metastatic versus non-metastatic cell lines (Fig. 2e). When comparing receptor negative primary cancer cells versus cells obtained from metastatic TNBCs, we often observed increased propionyl CoA carboxylase (PCC) expression (Fig. 2e, Extended Data Fig. 1a),

although this was not induced by TGF β /TNF α during the time frame we have studied. These data implicate the conversion of the D- to L-isomer of methylmalonyl-CoA as the common point of disruption in propionate metabolism by TGF β /TNF α and the likely source of increased MMA production during metastatic signaling. Importantly, this observation is not specific to TNBCs as treatment of lung adenocarcinoma cells (A549) with TGF β /TNF α , which promotes the acquisition of metastatic properties in these types of cancer, also promoted increased accumulation of MMA, which correlated with suppression of MCEE expression (Extended Data Fig. 1b–c). In accordance with the importance of MCEE expression levels for TNBC metastasis, analysis of publicly available databases shows that low expression of MCEE in lymph node positive TNBC tracks with significantly reduced survival and poor prognosis (Extended Data Fig. 1f–g). Combined, these data indicate that MCEE is the point of propionate metabolism deregulation by metastatic inducers and an important metabolic regulatory node in TNBCs.

Next, we sought to understand how MCEE expression is regulated by metastatic signaling. Much of the metastatic process stems from alterations in gene expression driven by transcriptional reprogramming^{13,14}, therefore we asked if reduced MCEE expression was the result of altered transcription. In support of this idea, MCEE mRNA levels were downregulated upon treatment with TGF β /TNF α (Fig. 2f–g). A marked loss of MCEE promoter activity confirmed that the suppression of MCEE protein levels in MCF10A and A549 cells by TGF β /TNF α was transcriptional (Fig. 2h, Extended Data Fig. 1d). Upon analysis of the MCEE promoter region, we found overlapping EGR1/SP1 binding sites, which are both downstream effectors of ERK (Fig. 2i). We have previously demonstrated that overlapping EGR1/SP1 binding sites can function as a switch downstream of ERK2 signaling. Upon ERK2 signaling, phosphorylated SP1, a positive regulator of this promoter, becomes dephosphorylated and EGR1, a negative regulator of this promoter that is dramatically induced, replaces SP1 and promotes transcriptional repression¹³. To determine if a similar mechanism could be at play, we used an ERK2 D319N-induced model of metastatic signaling in MCF10A cells^{15,16}. As in the TGF β /TNF α induced breast and lung cancer cells, we saw that ERK2 D319N expression suppressed expression of MCEE compared to control cells, while markedly increasing MMA levels (Fig. 2j–k). Importantly, in this ERK2 D319N-overexpressing system, MCEE promoter activity was also suppressed, supporting an ERK2-driven transcriptional regulation at the overlapping EGR1/SP1 binding sites (Fig. 2l). Knockdown of SP1 in both MCF10A and HCC1806 cells mimicked ERK2-mediated suppression of MCEE (Fig. 2m). Additionally, a phospho-mimetic mutant of SP1 was able to rescue MCEE expression in ERK2-induced MCF10A cells, whereas wild-type SP1 and a non-phosphorylatable form of SP1 maintained suppression, despite induction of EGR1 (Fig. 2n). In accordance with this model, inhibition of ERK suppressed the ability of TGF β /TNF α to induce EGR1 and SP1 dephosphorylation and concomitantly also blocked TGF β /TNF α mediated repression of MCEE expression (Fig. 2o). Together, our data support a mechanism in which metastatic signaling, dependent on ERK, promotes MMA production by creating an environment where phosphorylated SP1, a positive regulator of MCEE expression, becomes dephosphorylated and is replaced by EGR1 in the promoter region of MCEE, antagonizing MCEE expression.

To support our findings highlighting the link between dysregulation of propionate metabolism to metastatic progression, we utilized a genetic approach. MCEE knockdown, which mimicked its suppression by metastasis inducers and resulted in increased MMA levels (Extended Data Fig. 2a–b), was sufficient to regulate expression of pro-aggressive markers associated with cancer progression, including loss of epithelial and gain of mesenchymal markers, in MCF-10A, HCC1806 and A549 cells (Extended Data Fig. 2c). We next sought to resolve whether increasing MMA through alteration of other points of the propionate metabolism pathway could similarly increase metastatic aggressiveness. Toward this end, we knocked down MUT in A549, MCF-10A and HCC1806 cells, which also led to increased levels of MMA and, as in MCEE knockdown, pro-aggressive markers were altered (Fig. 3a–b, Extended Data Fig. 3a–c). We have previously shown that MMA is sufficient to induce a pro-metastatic gene expression profile⁵, and similarly, knockdown of MUT also induced a similar gene expression profile with metastatic characteristics, including increased expression of *SOX4*, *TFGB1*, *TGFBR1* and *TGFBR2* (Supplementary Table 2, Fig. 3c, Extended Data Fig. 3d–g). MMA levels have been reported to be increased in the serum of individuals with vitamin B12 deficiency, due to the requirement of vitamin B12 for MUT activity downstream of MCEE¹⁷. Indeed, depletion of vitamin B12 from the media also replicated this effect, as did knockdown of *MMAB*, the gene encoding the enzyme cob(I)alamin adenosyltransferase, which converts vitamin B12 to its biologically active form utilized by MUT (Extended Data Fig. 4a–e). To further determine if manipulation of propionate metabolism and MMA accumulation could promote cancer progression in mice, we knocked down MUT in a metastatic breast cancer cell line, MDA-MB-231 cells. Reduced expression of MUT in these cells increased MMA levels and increased the cells' capacity to migrate and invade in transwell assays (Figure 3d–f). We then demonstrated that these cells had increased ability to colonize and grow in lungs of mice following a tail-vein injection (Fig 3g–h).

PCC catalyzes the carboxylation of BCAA and OCFA-derived propionyl-CoA into D-methylmalonyl-CoA and therefore regulates flux through the propionate metabolic pathway and the ability to generate MMA (Fig. 1c). In accordance with this, overexpression of PCC resulted in increased propionyl-CoA levels and consequently increased flux through the propionate metabolic pathway, as demonstrated by an increase in MMA and succinate as well as other TCA cycle intermediates (Extended Data Fig. 5a–f). Mirroring its effects on MMA levels, overexpression of PCC in HCC1806, MCF-10A and A549 cells promoted pro-metastatic markers (Extended Data Fig. 5g). While PCC overexpression did not have a significant effect on the migratory ability of cells, it significantly increased invasion ability and lung colonization following tail vein injection of MDA-MB231 cells (Extended Data Fig. 5h–k). Further supporting the importance of PCC for the endogenous production of MMA in cancer cells, knockdown of PCCA (one of the subunits of the PCC enzyme complex necessary for its function) abrogates TGF β /TNF α -mediated increase in MMA levels (Fig. 4a). Importantly, knockdown of PCCA, while having no effect by itself in pro-aggressive markers in non-metastatic cancer cells, was sufficient to partially block TGF β /TNF α -induced pro-aggressive properties in these cells (Fig. 4b, Extended Data Fig. 6a–b, 6d). However, PCCA knockdown had no effect in the induction of pro-aggressive properties induced by exogenous MMA treatment (Fig. 4d, Extended Data Fig. 6c),

further supporting the dependence on MMA for PCC-mediated regulation of pro-aggressive properties. Finally, a MDA-MB-231 cell line clone has been isolated with greatly increased ability to colonize and grow in lungs, MDA-MB-231-LM2¹⁸. Interestingly, MDA-MB-231-LM2 cells show an increase in MMA levels compared to its parental line (Extended Data Fig. 3h) which has less ability to effectively form metastatic colonies¹⁸. Knockdown of PCC in these cells dramatically suppressed their metastatic potential, affecting their expression of mesenchymal markers in an MMA-dependent manner, inhibiting their ability to migrate and invade in transwells assays (Fig. 4c–f), a phenomenon also observed in another cell line with high metastatic potential (Hs578T; Extended Data Fig. 6e–g), and reducing their capacity to colonize the lungs of mice (Fig. 4g–h). PCCA knockdown in the highly metastatic cell lines MDA-MB-231-LM2 and Hs578T also affected their ability to proliferate (Extended Data Fig. 6h–i). Although we cannot discard the possibility that this effect may be influenced by changes in TCA cycle intermediates unrelated to MMA levels, together, our data reveal an important regulatory role of PCC in the endogenous production of MMA by cancer cells and suggest that PCC might constitute a valuable therapeutic target for metastatic TNBC.

We have recently reported that the metabolite MMA represents a vital link between aging and the severity of cancer prognosis⁵. Now, we demonstrate that cancer cells themselves are able to increase MMA levels by altering propionate metabolism in highly aggressive cancers such as TNBCs, allowing them to undergo a pro-metastatic reprogramming. Through transcriptional inhibition of MCEE, flux through propionate metabolism was impeded, resulting in accumulation of MMA. Together, we reveal a strategy utilized by cancer cells to acquire the aggressive traits and capabilities imperative to the progression of disease, centered around the accumulation of an endogenous metabolic byproduct. While the dysregulation of propionate metabolism to accumulate MMA within the tumor, and the revelation of its dual roles as both a tumor-produced as well as an age-associated systemic oncometabolite, underscores the significance of MMA in cancer, many questions remain to be elucidated. Does the MMA produced by tumor cells function primarily in an autocrine fashion, or can it also be secreted to act upon neighboring tumor cells and other cell types? How does MMA regulate the transcriptional program that underlies metastatic ability? At this point in our venture, there is still much to be uncovered about this previously disregarded metabolite. Our findings provide a foundation for further research that will conceivably widen the scope of our understanding of metabolic reprogramming in the tumor microenvironment, aging, and cancer.

Methods

Email contact for reagent and resource sharing: ana.gomes@moffitt.org and job2064@med.cornell.edu

Cell Lines

All human breast epithelial and cancer cell lines were obtained from the American Type Culture Collection (ATCC). MCF-10A (ATCC: CRL-10317) cells were cultured were cultured in DMEM:F12 media (Corning) supplemented with 5% horse serum (Gibco), 20 ng/mL EGF (Peprotech), 100 ng/mL cholera toxin (Sigma-Aldrich), 10 µg/mL insulin

(Sigma-Aldrich), 0.5 mg/mL hydrocortisone (Sigma-Aldrich) and penicillin-streptomycin (Gibco). SKBR3 (ATCC: HTB-30) cells were maintained in McCoy's 5a (Corning) media supplemented with 10% FBS (Sigma-Aldrich). MCF-7 (ATCC: HTB-22), T47D (ATCC: HTB-133) and BT-549 (ATCC: HTB-122) cells were cultured in RPMI-1640 (Corning) medium supplemented with 10% FBS and 0.01 mg/ml insulin (Sigma-Aldrich) for MCF7 and T47D, and 0.001 mg/ml insulin for BT-549. A549 (ATCC: CCL-185), HCC1806 (ATCC: CRL-2335), BT-20 (ATCC: HTB-19), HCC38 (ATCC: CRL-2314), MDA-MB-231 (ATCC: HTB-26) and MDA-MB-436 (ATCC: HTB-130) cells were cultured in RPMI-1640 medium supplemented with 10% FBS. Hs578T (ATCC: HTB-126) cells were maintained in high glucose DMEM (Gibco) with 0.01 mg/ml insulin and 10% FBS. MDA-MB-231-luciferase parental and metastatic LM2 subclone cells, described previously¹⁸, were obtained from Dr. Massague's lab and were maintained in high glucose DMEM supplemented with 10% FBS. HEK293T cells were obtained from GenHunter and cultured in high glucose DMEM supplemented with 10% FBS. Mouse breast cancer cell line clones 4T1, the metastatic one, and the locally invasive clone 4TO7 were originally derived by Dr. F. Miller¹⁹ and obtained from Dr. William Schiemann. They were maintained in RPMI-1640 with 10% FBS. All cell lines were maintained at 37°C and 5% CO₂ in the presence of 100 unit/ml penicillin and 100 µg/ml streptomycin (Gibco). All cell lines were routinely tested for mycoplasma and were at all times mycoplasma negative.

Mice

Female nu/nu athymic mice were purchased from Envigo at the age of 4–6 weeks. Xenograft experiments were started 7–10 days after the mice were received. The maximum tumor size allowed by Weill Cornell Medicine institutional review board is 20 mm or 2.5 cm³, or 10% of the animal's body weight, and this maximum size was not exceeded. The mice were maintained at Weill Cornell Medicine in compliance to Weill Cornell Medicine Institutional Animal Care and Use Committee protocols. Mice were maintained under standard husbandry conditions, group housed (5 maximum) in conventional cages with unrestricted food and water access. The room was maintained at 21–23 °C, around 50% humidity and a 12 hours light-dark cycle. PicoLab Rodent Diet 5053 (Labdiet, Purina) containing 20% protein and 5% fat was used. Mice were monitored by staff daily to observe health, maintain food and water and ensure cage cleanliness. BALB/cOlaHsd mice were purchased from Envigo and were maintained at KU Leuven/VIB in compliance with local ethical regulations and all experiments were approved by the KU Leuven ethics committee. The animals were maintained with unrestricted food and water access under 14h light, 10h dark cycle at 22±2 °C and between 45–70% humidity. The mice were fed Ssniff Rodent Diet containing 19% protein and 3.3% fat. Experiments started when mice were 6 week old and the maximum tumor size allowed by the ethics committee was not exceeded. The experiments concluded when the tumors reached 1.8 cm³ or got ulcerated.

METHOD DETAILS

Cell Culture Treatments

Cells were treated with 5 ng/ml of recombinant human TGF-β1 (PeproTech) and 5 ng/ml of recombinant human TNFα (PeproTech) to induce EMT for the indicated time period

up to 10 days. For MMA treatments, cells were treated with 5 mM MMA (Tocris) for the indicated times. For vitamin B12 depletion, cells were maintained in custom media missing vitamin B12. The custom media was prepared by Media Preparation Core at Memorial Sloan Kettering Cancer Center.

Targeted Metabolomics and Data Analysis

Metabolites were harvested, extracted and analyzed as described before²⁰. In short, the primary tumor and lung metastases were collected, washed in ice cold blood bank saline, dried on a sterile compress and frozen using a liquid nitrogen cooled Biosqueezer (Biospec Products) as fast as possible. The tissues were stored at -80°C until further extraction of the metabolites. For extraction of the metabolites, tissues were weighed and pulverized (Cryomill, Retsch) under liquid nitrogen conditions. The pulverized tissues were extracted with 800 μL of 62.5% methanol containing glutaric acid as an internal standard and 500 μL of precooled chloroform. Samples were vortexed at 4°C for 10 min and centrifuged at max speed for 10 min at 4°C . After centrifugation, phase separation was achieved, after which the methanol/water (upper) phase was separated and dried by vacuum centrifugation at 4°C . Targeted liquid chromatography-tandem mass spectrometry (LC-MS/MS) was performed using a 5500 QTRAP triple quadrupole mass spectrometer (AB/SCIEX) coupled to a Prominence UFLC HPLC system (Shimadzu) with Amide HILIC chromatography (Waters). Data were acquired in selected reaction monitoring (SRM) mode using positive/negative ion polarity switching for steady-state polar profiling of greater than 260 molecules. Peak areas from the total ion current for each metabolite SRM transition were integrated using MultiQuant v2.0 software (AB/SCIEX). Statistical analysis of the data was carried out using MetaboAnalyst, a free online software for the analysis of metabolomic experiments (www.metaboanalyst.ca, v4.0). The original peak intensity was normalized to the mean of the entire metabolome in each sample and log transformed prior to further analysis (Table S1).

Methylmalonic Acid, Propionyl-CoA and TCA cycle intermediate levels and tracing

Methylmalonic acid and other polar metabolites (including propionyl-CoA, succinate, fumarate, malate and oxaloacetate) were extracted from cells in culture using 80% (v/v) aqueous methanol as described before for polar metabolite extraction²¹ and measured by targeted LC-MS/MS using the same method as described above for targeted metabolomics. For ^{13}C tracing experiments, HCC1806 cells were treated with TGF- β and TNF α as described above for 24 hours after which the medium was changed to either glucose and glutamine free RPMI containing 2 g/L [^{13}C]glucose, 300 mg/L [^{13}C]glutamine and 10% dialyzed serum or valine, isoleucine, threonine and methionine free RPMI containing 20 mg/L [^{13}C]valine, 50 mg/L [^{13}C]isoleucine, 20 mg/L [^{13}C]threonine, 15 mg/L [^{13}C]methionine and 10% dialyzed serum for an additional 48 hours. TGF- β and TNF α treatments were maintained through the course of the labeling timeline. Metabolites were extracted and analyzed by LC-MS/MS as described above. The original peak intensity was normalized to protein levels. Data are represented as relative peak intensity as no absolute quantitation was performed.

Gene Silencing

shPCCA #1 (TRCN0000078424), shPCCA #2 (TRCN0000078427), shMMAB #1 (TRCN0000083905), shMMAB #2 (TRCN0000083904), shMCEE #1 (TRCN0000049481), shMCEE #2 (TRCN0000049482), shMUT #1 (TRCN0000049038), shMUT #2 (TRCN0000049042), shSP1 #1 (TRCN0000285151), shSP1 #2 (TRCN0000274208) and shNT (shGFP - TRCN0000072181) (all from Sigma Aldrich) lentiviruses were produced in HEK293T cells by co-transfecting each with plasmids encoding psPAX2 (Addgene plasmid 12260), and pMD2.G (Addgene plasmid 12259) using X-tremeGENE HP (Roche) following the manufacturer's protocol. Media was changed 24 hours post-transfection and the viruses were harvested 48 hours after the media change. Cells were transduced with the filtered virus in the presence of 8 µg/mL polybrene (Sigma-Aldrich). Selection of resistant cells was initiated 24 hours later using 2 µg/mL puromycin (Sigma-Aldrich), and transduced cells were maintained with 2 µg/mL puromycin (Sigma-Aldrich) in their growth media for the duration of the experiments.

Generation of Stable Overexpressing Cell Lines

Human PCCA and PCCB open reading frame clones were obtained from the human ORFeome collection (PlasmidID, Harvard Medical School) and GFP was obtained from Addgene (Addgene plasmid 15301) in the Gateway compatible pDONR223 vector. These DONR vectors were then recombined into the Gateway destination vector PHAGE C-TAP (a kind gift from Dr. Wade Harper²²) using LR clonase II (Thermo Scientific). PHAGE C-TAP lentiviruses were produced the same way as described above. To overexpress PCC, equal amounts of PCCA and PCCB expressing virus was used. The virus particles for mutant SP1 and pInducer20 GFP, ERK2 D319N constructs¹³ were produced by co-transfection of HEK293T cells with plasmids encoding psPAX2 (Addgene plasmid 12260), and pMD2.G (Addgene plasmid 12259) using X-tremeGENE HP (Roche) in accordance with the manufacturer's protocol. All cells were transduced in the presence of 8 µg/mL polybrene (Sigma-Aldrich), and the selection of resistant cells was initiated 24 hours later using the appropriate antibiotic marker (2 µg/mL puromycin or 300 µg/mL G418 (Sigma-Aldrich)). Transduced cells were maintained for the time points indicated. Cells carrying the inducible GFP or ERK2 D319N transgenes were maintained un-induced in culture. To induce the expression of the transgenes, the cells were treated daily with 0.5 µg/mL doxycycline for the time points indicated.

Proliferation Assays

MDA-MB-231 LM2 metastatic clone or Hs578T cells with knockdown of PCCA for 3 days were seeded on 96-well plates. The plates were placed in the Incucyte Live Cell Imaging system and kept at 37 °C and 5% CO₂ for the duration of the experiment. The imaging started 4 hours after seeding and images were taken every 8 hours. Proliferation of the cells over time was measured as increase in confluency, which was done by image analysis using the Incucyte software (v. 2021A).

Transwell Migration and Invasion Assays

Luciferase-expressing parental MDA-MB-231 cells¹⁸ with knockdown of MUT for 6 days or with PCC overexpression for 6 days, or metastatic clone MDA-MB-231 LM2 cells with knockdown of PCCA for 6 days, or Hs578T cells with knockdown of PCCA for 6 days were used in transwell migration and invasion assays²³. For migration assays, Boyden chamber inserts (BD Biosciences, 8 µm pore size) were pre-coated with 25 µg/µl rat tail collagen 1 (Corning). For cell invasion assays, BD BioCoat invasion chambers coated with growth factor reduced Matrigel were used. Invasion chambers were prepared according to manufacturer's specifications. For both migration and invasion assays, cells (5×10^4 cells/ 250 µl assay media) were then added to the top chamber of cell culture inserts in a 24-well companion plate. High-glucose DMEM (Gibco) supplemented with 250 µg/mL BSA (Sigma-Aldrich) was used as the assay media, and high glucose DMEM media supplemented with 10% FBS (Sigma-Aldrich) (and 0.01 mg/ insulin for Hs578T cells) was used as the chemoattractant for both migration (6 hours) and invasion assays (20 hours). After the indicated incubation, the cells that had migrated/invaded to the lower surface of the membrane were fixed with ethanol and stained with 0.2% crystal violet in 2% ethanol.

Images of crystal violet stained cells were captured using a Nikon DS-Fi2 camera, and quantification were carried out in an automated way using Fiji/ImageJ (v1.52 or v1.53n). Briefly, binary images of the area covered by crystal violet-positive cells was generated using thresholding and settings that were appropriate for control samples, and these settings were used throughout the analysis. The percentage area covered by crystal violet-positive cells was quantified for each condition, using a minimum of two technical replicates.

Immunoblots for Total Cell Lysates

Cell lysates were prepared using acid extraction with 10% TCA solution (10% trichloroacetic acid, 25 mM NH₄OAc, 1 mM EDTA, 10 mM Tris·HCl pH 8.0). Precipitated proteins were resolubilized in a 0.1 M Tris·HCl pH 11 solution containing 3% SDS and boiled for 10–15 minutes. 20 µg total protein per sample as determined with the DC Protein Assay kit II (BioRad) were run on SDS-PAGE under reducing conditions. The proteins were transferred from the gels to nitrocellulose membranes (GE Healthcare) electrophoretically and then the membranes were blocked in TBS-based Odyssey Blocking buffer (LI-COR). Membranes were incubated with the primary antibodies overnight at 4°C. The antibodies used to detect the proteins of interest were: E-Cadherin (610181 - BD Biosciences, Dilution 1:1000), Fibronectin (ab2413 - Abcam, Dilution 1:5000), Vimentin (5741S - Cell Signaling, Dilution 1:1000), Serpine1 (612024 - BD Biosciences, Dilution 1:1000), CTGF (ab6992 - Abcam, Dilution 1:1000), CXCR4 (ab124824 - Abcam, Dilution 1:1000), MMP2 (4022S - Cell Signaling, Dilution 1:1000), HA (sc-7392 - Santa Cruz, Dilution 1:5000), EGR1 (ab133695 - Abcam, Dilution 1:1000), SP1 pS739 (ab195733 - Abcam, Dilution 1:500), SP1 (39058 - Active Motif, Dilution 1:1000), ERK1/2 (9102L - Cell signaling, Dilution 1:5000), ERK1/2 pT202/pY204 (4370L - Cell Signaling, Dilution 1:2000), MMP9 (3852S - Cell Signaling, Dilution 1:1000), MCEE (19499-1-AP - Proteintech, Dilution 1:250), MMAB (ab174831 - Abcam, Dilution 1:500), MUT (ab134956 - Abcam, Dilution 1:1000), PCCA (ab187686 - Abcam, Dilution 1:1000), PCCB (HPA036940 - Sigma-Aldrich, Dilution 1:1000) and Actin (sc1615 - Santa Cruz, Dilution 1:10,000). The membranes

were then incubated with the appropriate horseradish peroxidase–conjugated (HRP) anti-rabbit (NA934–Cytiva, Dilution 1:10,000), anti-mouse (NA931–Cytiva, Dilution 1:10,000), or anti-goat (AP180P–Millipore, Dilution 1:10,000) immunoglobulin for 2 hours at room temperature. The signals were developed using Amersham ECL detection system (GE Healthcare).

MCEE Promoter Activity

MCEE promoter activity was evaluated using a luciferase-based promoter construct (Genecopoeia, HPRM51389). MCF-10A cells treated with TGF β 1-TNF α , or expressing GFP or ERK2 D319N for 1 day were transfected with the MCEE promoter using XtremeGENE HP (Roche) in accordance with the manufacturer’s protocol. The day after the transfection the media was replaced, and TGF β 1-TNF α treatment or doxycycline for the expression of GFP or ERK2 D319N maintained in the media. A549 cells treated with TGF β 1-TNF α were similarly prepared. Luciferase activity was measured at day 3 of treatment or expression using a Secrete-Pair Dual Luminescence Assay Kit (Genecopoeia, LF032) according to the manufacturer’s instructions on an Envision plate reader (PerkinElmer). The data are presented normalized to the secreted alkaline phosphatase signal to normalize for variation between transfection replicates.

Gene Expression Analysis

RNA was extracted from cell lines using the PureLink RNA isolation kit (Life Technologies) and DNase I (Amplification grade, Sigma-Aldrich) treatment was utilized to digest contaminating DNA. Using iSCRIPT cDNA synthesis kit (BioRad) cDNA was synthesized and quantitative PCR (qPCR) using SYBR green master mix (Life Technologies) was performed on a QuantStudio6 Real-Time PCR system (Life Technologies, software version v1.3). Target gene expression was normalized to beta actin and Tata Binding Protein (TBP) expression. Primer sequences can be found in the following table:

Global Gene Expression Analysis (RNA-sequencing)

Total RNA was extracted from A549 cells with MUT knockdown for 3 days as described above. The extracted RNA was sent to Active Motif for further processing and RNA-seq analysis. Briefly, RNA quality was assessed by BioAnalyzer, and the RIN values for all samples were 10.0. Directional Poly-A RNA-seq libraries were prepared and sequenced as PE42 (42-bp paired-end reads) on Illumina NextSeq 500 to a depth of 34.0–49.0M read pairs. The “TopHat” algorithm v2.1.0 (Bowtie v2.2.6.0) was used to align the reads to the hg38 genome which was obtained from iGenomes (https://support.illumina.com/sequencing/sequencing_software/igenome.html). The alignments (31.3–46.2M aligned pairs) in the BAM files were further analyzed using the Cufflinks suite of programs v2.2.1 (running consecutively: Cufflinks (2.2.1.Linux_x86_64) Cuffcompare (v2.2.1) Cuffdiff (v2.2.2). Cufflinks was run using the hg38-genes as a reference database. The cufflinks outputs were compared using cuffdiff. The accession number for the raw sequencing data reported in this paper is GEO: GSE161108. Gene set enrichment using GSEA software^{24,25} (v.4.0.3) was performed on genes that were significantly changed 1.5 fold. “Classic” enrichment statistics and “ratio of classes” metrics were used for analysis. Number of permutations were set to 1000 as suggested, and “gene set” was used as permutation type. Gene Ontology

(GO)-Biological Processes (BP) gene set database from the Molecular Signatures Database (MSigDB) collection v6.2 was utilized.

Lung Colonization in Mice

100,000 cells in 100 μ L PBS—luciferase-expressing parental MDA-MB-231 cells¹⁸ with knockdown of MUT for 6 days or with PCC overexpression for 6 days, or metastatic MDA-MB-231 LM2 clone with knockdown of PCCA for 6 days—were injected into the tail veins of 7 week old female nu/nu athymic mice. 7–10 mice were used in each experimental group. Lung colonization was evaluated as described before^{18,26} by utilizing IVIS Spectrum CT Pre-Clinical In Vivo Imaging System (Perkin-Elmer) to monitor the metastases. To determine lung colonization, the luminescence was measured and quantified 6 weeks after the injections using the Living Image Software (v4.5, Perkin-Elmer). All animal studies followed the guidelines of and were approved by the Weill Cornell Medicine Institutional Animal Care and Use Committee.

4T1 Syngeneic Orthotopic Tumor Mouse Model

Six-week-old female BALB/c mice were inoculated with 1×10^6 4T1 cells in a volume of 50 μ L PBS in the mammary fat pad. After four days, a primary tumor nodule was already established. Mice were sacrificed 21 days after cancer cell injection with an overdose of Dolethal (140 mg/kg, 2.8 μ L per gram of animal weight of a 50 mg/ml solution). The animal study complies with ethical regulations and was approved by the KU Leuven ethics committee.

Statistical Analysis

Data analyses were performed using Microsoft Excel 2013 or 365 and GraphPad Prism 7 or 9. A two-tailed paired Student's t test was used to determine significance when two conditions were compared; for experiments with more than two conditions a one-way or two-way ANOVA as indicated in figure legends was used to determine significance. In both types of statistical analyses values of $p < 0.05$ were considered significant. Data are represented as the mean \pm SEM (standard error of the mean) of individual data points, and the mean \pm SEM of at least three independent experiments performed. Number of replicates and animals are reported in the figure legends. For all experiments similar variances between groups were observed. Normal distribution of samples was not determined. In the GSEA analysis FDR corrected p values are used to determine significance.

Data Availability

Source data information for the metabolomics experiment can be found on Supplementary Table 1. RNA sequencing data that support the findings of this study have been deposited in the Gene Expression Omnibus (GEO) under the accession code GSE161108, as well as summary information in Supplementary Table 2. The raw data supporting each figure and the raw images for the western blots can be found in the corresponding Source Data files.

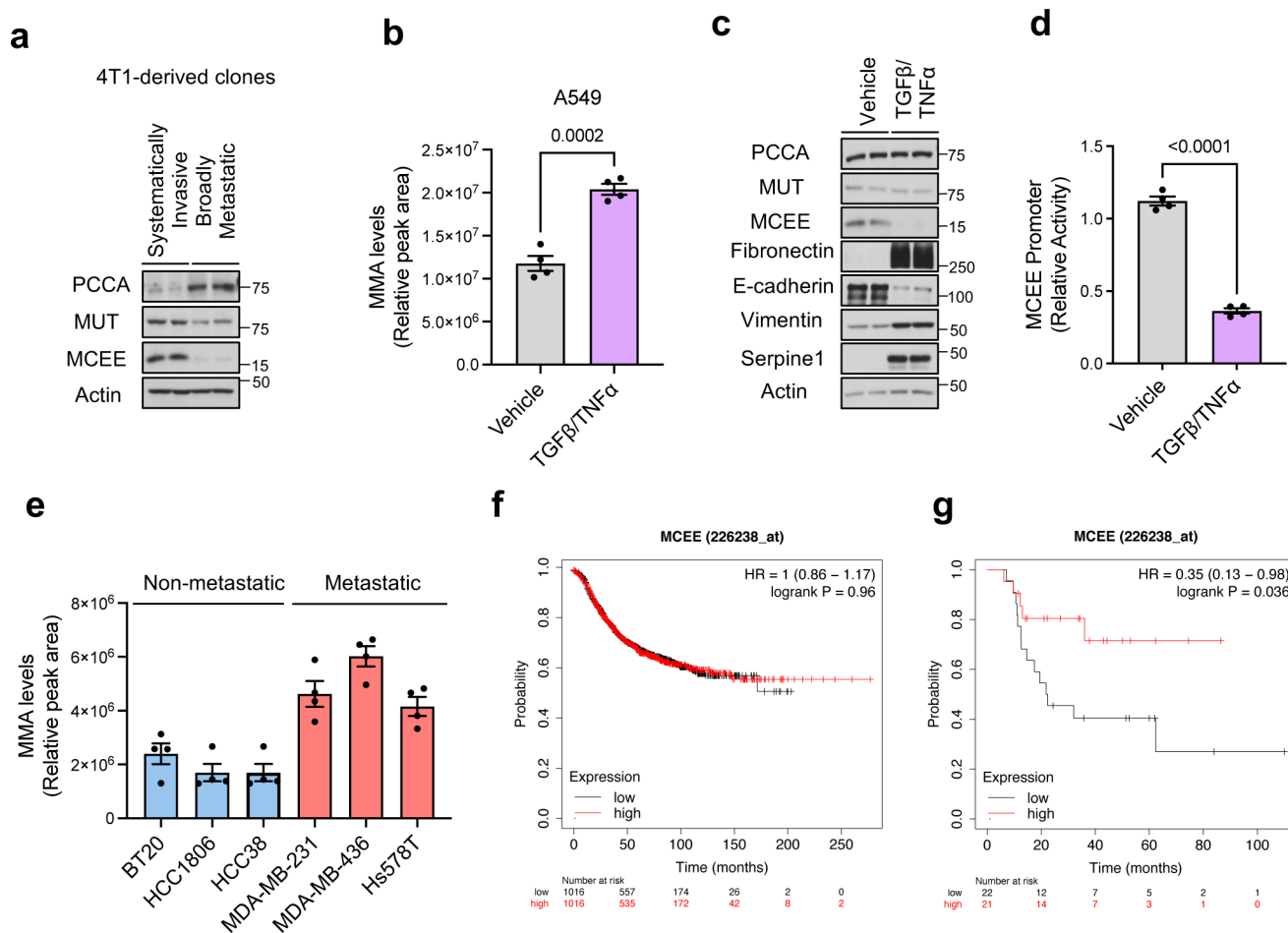
For RNA-seq analysis, the hg38 reference genome database was obtained from iGenomes (https://support.illumina.com/sequencing/sequencing_software/igenome.html)

and the GSEA analysis was done with gene sets derived from the GO biological processes gene sets in the Molecular Signatures Database (MSigDB) collection v6.2, which can be accessed through <https://www.gsea-msigdb.org/gsea/msigdb/index.jsp>.

Code Availability

Fiji/ImageJ macro for automation of quantification of transwell migration and invasion assays is not a standalone code but is available from the corresponding authors upon reasonable request.

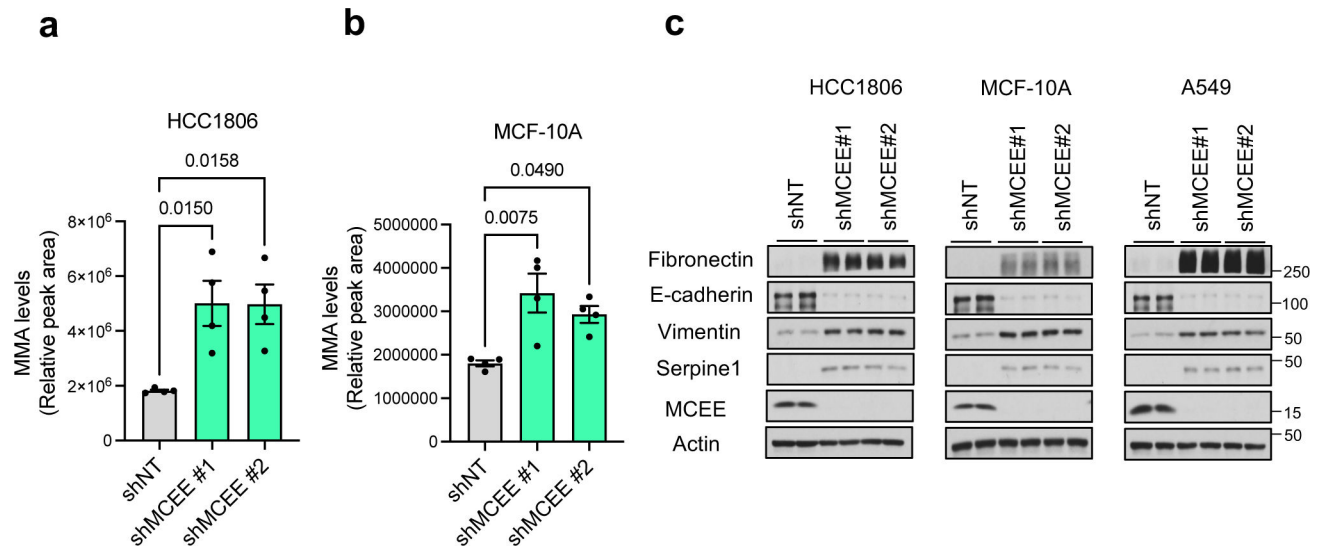
Extended Data



Extended Data Fig. 1. Methmalonic acid and MCEE levels are altered by metastatic signaling in different cancer cell models.

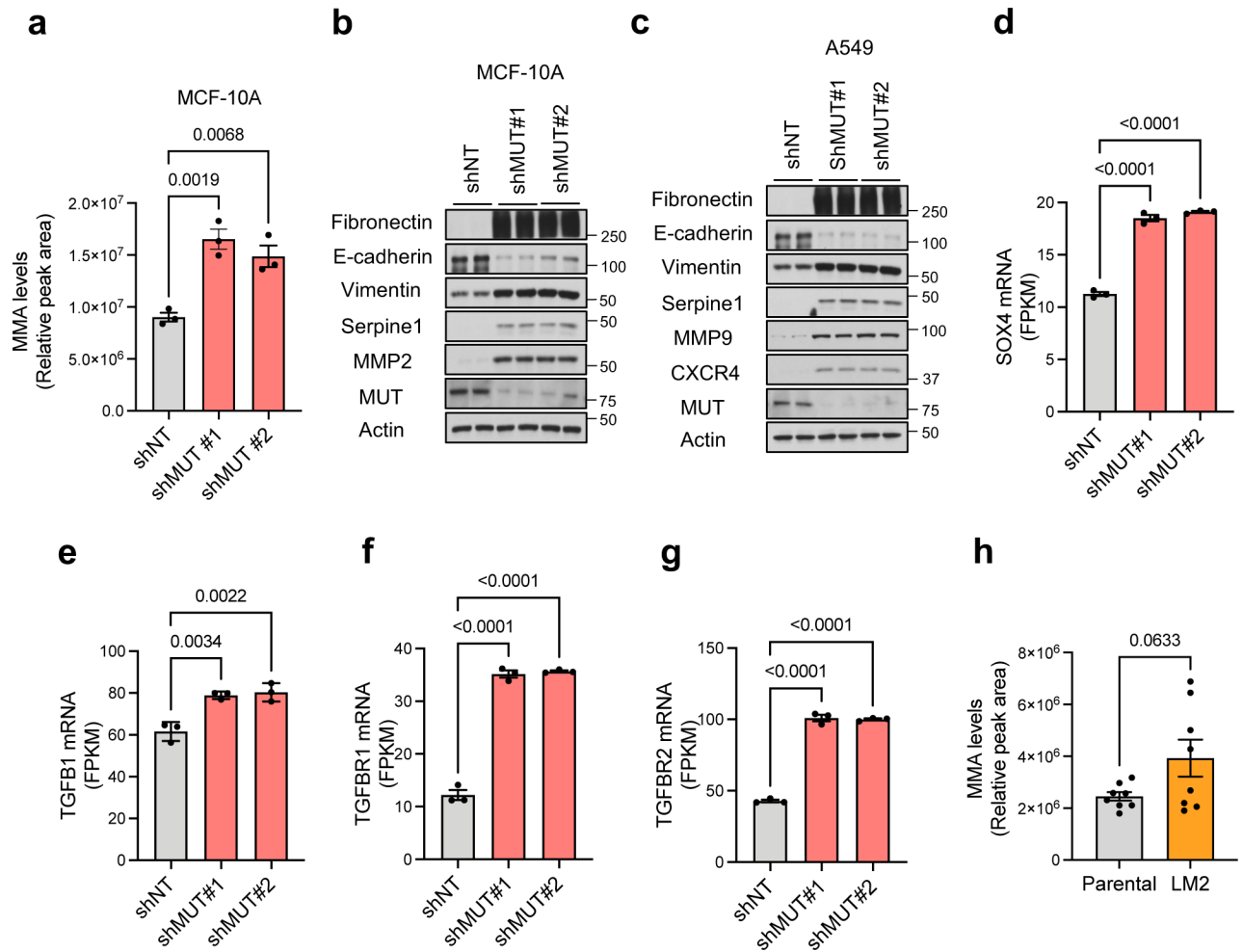
(a) Propionate metabolism-related enzyme levels evaluated by immunoblots in 4T1-derived clones of cells with different metastatic potential; representative images (n=4). (b) MMA levels in A549 cells treated with TGFβ + TNFα for 3 days (n=4, two-tailed *t*-test). (c) Propionate metabolism-related enzyme levels evaluated by immunoblots in A549 cells treated with TGFβ + TNFα for 3 days; representative images (n=4). (d) MCEE-luciferase promoter activity in A549 cells treated with TGFβ + TNFα for 3 days (n=4, two-tailed

t-test). **e**, MMA levels in non-metastatic and metastatic triple negative breast cancer human cell lines (n=4). **f**, Kaplan-Meier survival curve of breast cancer patients as a function of MCEE expression. **g**, Kaplan-Meier survival curve of lymph node positive triple negative breast cancer patients as a function of MCEE expression. All values are expressed as mean \pm SEM.



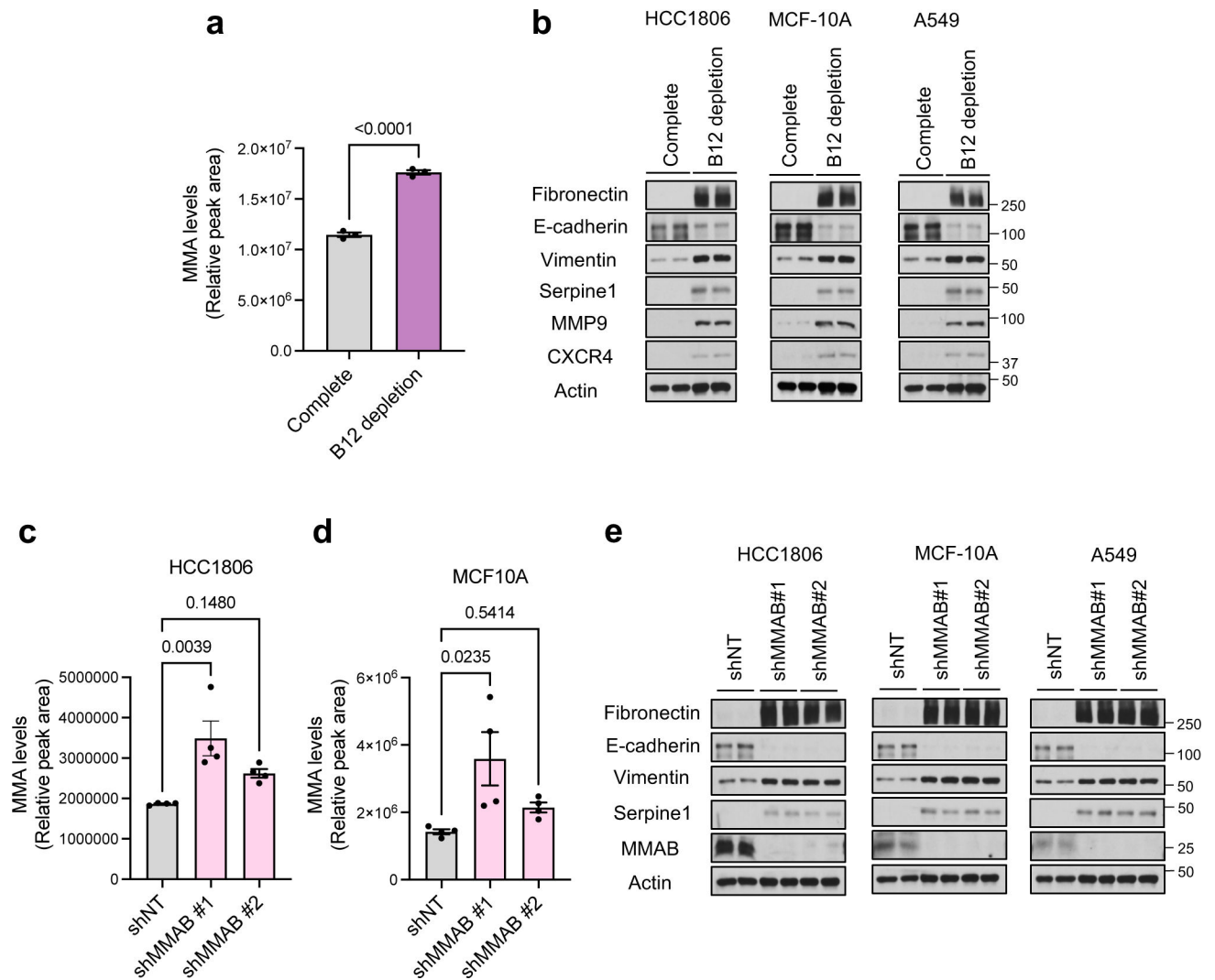
Extended Data Fig. 2. Knockdown of MCEE induces a pro-aggressive reprogramming.

a, b, MMA levels in HCC1806 (**a**) and MCF-10A (**b**) cells with MCEE knockdown for 2 days (n=4, one-way ANOVA with Tukey's multiple comparison test). **c**, Immunoblots for EMT and aggressiveness markers in HCC1806, MCF-10A and A549 cells with MCEE knockdown for 10 days; representative images (n=4). All values are expressed as mean \pm SEM.

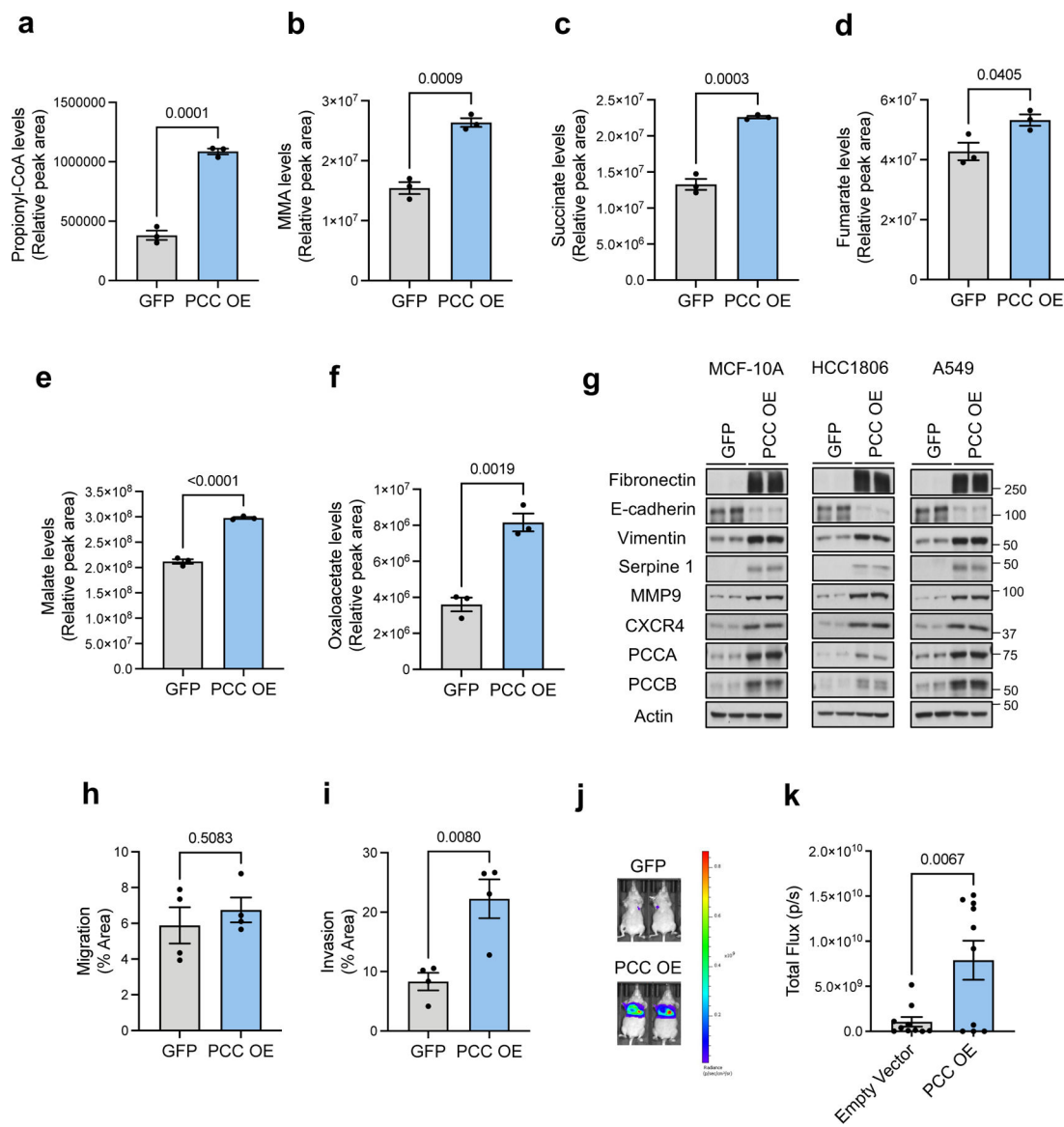


Extended Data Fig. 3. Suppression of MUT induces a pro-aggressive reprogramming.

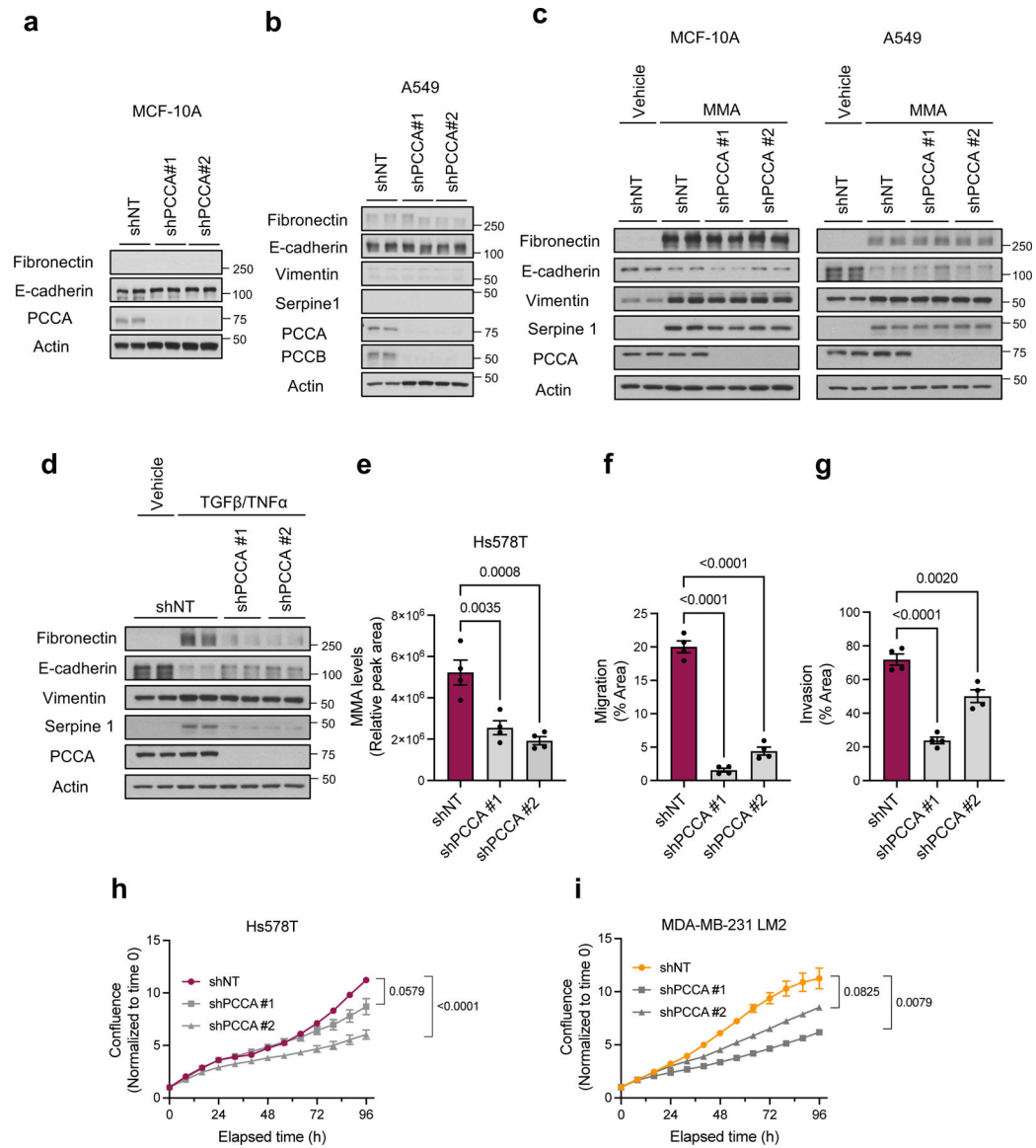
a, MMA levels in MCF-10A cell with MUT knockdown for 3 days ($n=3$, one-way ANOVA with Tukey's multiple comparison test). **b**, **c**, Immunoblots for EMT and aggressiveness markers in MCF-10A (**b**) and A549 (**c**) cells with MUT knockdown for 10 days; representative images ($n=4$). **d**, **e**, **f**, **g**, mRNA levels of SOX4 (**d**), TGFB1 (**e**), TGFB1 (**f**), and TGFB2 (**g**) evaluated by RNA sequencing in A549 cells with MUT knockdown for 3 days ($n=3$, one-way ANOVA with Tukey's multiple comparison test). **h**, MMA levels in MDA-MB-231-LM2 versus MDA-MB-231-luciferase parental cells ($n=8$, two-tailed t -test). All values are expressed as mean \pm SEM.



Extended Data Fig. 4. Vitamin B12 deficiency induces a pro-aggressive reprogramming.
a, MMA levels in MCF-10A cells grown in complete or Vitamin B12-depleted media for 9 days (n=3, two-tailed *t*-test). **b**, Immunoblots for EMT and aggressiveness markers in HCC1806, MCF-10A and A549 cells grown in complete or Vitamin B12-depleted media for 10 days; representative images (n=4). **c**, **d**, MMA levels in HCC1806 (n=4) (**c**) and MCF-10A (n=4) (**d**) cells with MMAB knockdown for 3 days (one-way ANOVA with Tukey's multiple comparison test). **e**, Immunoblots for EMT and aggressiveness markers in HCC1806, MCF-10A and A549 cells with MMAB knockdown for 10 days; representative images (n=4). All values are expressed as mean ± SEM.



Extended Data Fig. 5. Overexpression of PCC induces a pro-aggressive reprogramming. **a, b**, Propionyl-CoA (**a**) and MMA (**b**) levels in MCF-10A cells overexpressing PCCA and PCCB for 5 days ($n=3$, two-tailed t -test). **c-f**, TCA cycle intermediates succinate (**c**), fumarate (**d**), malate (**e**), oxaloacetate (**f**) in MCF-10A cells overexpressing PCCA and PCCB for 5 days ($n=3$, two-tailed t -test). **g**, Immunoblots for EMT and aggressiveness markers in HCC1806, MCF-10A and A549 cells overexpressing PCCA and PCCB for 10 days; representative images ($n=4$). **h, i**, Transwell migration (**h**) and invasion (**i**) assays of MDA-MB-231-luciferase parental cells overexpressing PCCA and PCCB for 6 days ($n=4$, two-tailed t -test). **j, k**, Lung colonization assay of MDA-MB-231-luciferase parental cells injected after 6 days of PCCA and PCCB overexpression, imaged at 6 weeks; representative images (**j**) and quantification (**k**) ($n=10$, two-tailed t -test). All values are expressed as mean \pm SEM.



Extended Data Fig. 6. Knockdown of PCCA does not induce EMT.

a, b, Immunoblots for EMT markers in MCF-10A (**a**), and A549 (**b**) cells with PCCA knockdown for 10 days; representative images (n=4). **c**, Immunoblots for EMT markers in MCF-10A and A549 cells with PCCA knockdown and treated with 5 mM MMA for 10 days; representative images (n=4). **d**, Immunoblots for EMT markers in A549 cells with PCCA knockdown and treated with TGFβ + TNFα for 5 days; representative images (n=4). **e**, MMA levels in Hs578T cells with PCCA knockdown for 5 days (n=4, one-way ANOVA with Tukey's multiple comparison test). **f, g**, Transwell migration (**f**) and invasion (**g**) assays of Hs578T with PCCA knockdown for 5 days (n=4, one-way ANOVA with Tukey's multiple comparison test). **h, i**, Proliferation of Hs578T (**h**) and MDA-MB-231-LM2 (**i**) with PCCA knockdown for 5 days (n=4, two-way repeated measures ANOVA test based on general linear model (GLM) with Tukey's multiple comparison test, p values only shown for end point). All values are expressed as mean ± SEM.

Supplementary Material

Refer to Web version on PubMed Central for supplementary material.

Acknowledgments

We are grateful to members of the Blenis and Cantley Laboratories for critical input on this project. We are also thankful to Dr. William Schiemann for the 4T1 clones and Melanie Planque for experimental assistance. The Gomes Lab is supported by a Pathway to Independence Award to A.P.G. from NCI (R00CA218686), a New Innovator Award from OD/NIH (DP2 AG0776980) to A.P.G., the American Lung Association, the Florida Health Department Bankhead-Coley Research Program, the Florida Breast Cancer Foundation, and the George Edgecomb Society of Moffitt Cancer Center. T.S. is supported by the NIH F31 pre-doctoral fellowship F31CA220750. This research was supported by the NIH grant R01CA46595 and a research agreement with Highline Therapeutics to J.B. S.M.F. is funded by the European Research Council under the ERC Consolidator Grant Agreement number 711486 – MetaRegulation, FWO research grants and projects, KU Leuven Methusalem Co-funding and Fonds Baillet Latour.

Competing Interests Statement

S.M.F. has received funding from Bayer, Merck and BlackBelt Therapeutics and has consulted for Fund+. L.C.C. owns equity in, receives compensation from, and serves on the Board of Directors and Scientific Advisory Board of Agios Pharmaceuticals and Petra Pharma Corporation. No potential conflicts of interest were disclosed by the other authors.

References

1. Dillekas H, Rogers MS & Straume O Are 90% of deaths from cancer caused by metastases? *Cancer Med* 8, 5574–5576, doi:10.1002/cam4.2474 (2019). [PubMed: 31397113]
2. Mortality GBD & Causes of Death C Global, regional, and national life expectancy, all-cause mortality, and cause-specific mortality for 249 causes of death, 1980–2015: a systematic analysis for the Global Burden of Disease Study 2015. *Lancet* 388, 1459–1544, doi:10.1016/S0140-6736(16)31012-1 (2016). [PubMed: 27733281]
3. DeBerardinis RJ & Chandel NS Fundamentals of cancer metabolism. *Sci Adv* 2, e1600200, doi:10.1126/sciadv.1600200 (2016). [PubMed: 27386546]
4. Corrado M, Scorrano L & Campello S Changing perspective on oncometabolites: from metabolic signature of cancer to tumorigenic and immunosuppressive agents. *Oncotarget* 7, 46692–46706, doi:10.18632/oncotarget.8727 (2016). [PubMed: 27083002]
5. Gomes AP et al. Age-induced accumulation of methylmalonic acid promotes tumour progression. *Nature*, doi:10.1038/s41586-020-2630-0 (2020).
6. Tao K, Fang M, Alroy J & Sahagian GG Imagable 4T1 model for the study of late stage breast cancer. *BMC Cancer* 8, 228, doi:10.1186/1471-2407-8-228 (2008). [PubMed: 18691423]
7. Rinaldi G et al. In Vivo Evidence for Serine Biosynthesis-Defined Sensitivity of Lung Metastasis, but Not of Primary Breast Tumors, to mTORC1 Inhibition. *Mol Cell* 81, 386–397 e387, doi:10.1016/j.molcel.2020.11.027 (2021). [PubMed: 33340488]
8. Ngo B et al. Limited Environmental Serine and Glycine Confer Brain Metastasis Sensitivity to PHGDH Inhibition. *Cancer Discov* 10, 1352–1373, doi:10.1158/2159-8290.CD-19-1228 (2020). [PubMed: 32571778]
9. Spinelli JB et al. Metabolic recycling of ammonia via glutamate dehydrogenase supports breast cancer biomass. *Science* 358, 941–946, doi:10.1126/science.aam9305 (2017). [PubMed: 29025995]
10. Aslakson CJ & Miller FR Selective events in the metastatic process defined by analysis of the sequential dissemination of subpopulations of a mouse mammary tumor. *Cancer Res* 52, 1399–1405 (1992). [PubMed: 1540948]
11. Padua D & Massague J Roles of TGFbeta in metastasis. *Cell Res* 19, 89–102, doi:10.1038/cr.2008.316 (2009). [PubMed: 19050696]
12. Liu J, Lin PC & Zhou BP Inflammation fuels tumor progress and metastasis. *Curr Pharm Des* 21, 3032–3040, doi:10.2174/1381612821666150514105741 (2015). [PubMed: 26004407]

13. Gomes AP et al. Dynamic Incorporation of Histone H3 Variants into Chromatin Is Essential for Acquisition of Aggressive Traits and Metastatic Colonization. *Cancer Cell* 36, 402–417 e413, doi:10.1016/j.ccell.2019.08.006 (2019). [PubMed: 31564638]
14. Iwamoto T et al. Distinct gene expression profiles between primary breast cancers and brain metastases from pair-matched samples. *Sci Rep* 9, 13343, doi:10.1038/s41598-019-50099-y (2019). [PubMed: 31527824]
15. Shin S, Dimitri CA, Yoon SO, Dowdle W & Blenis J ERK2 but not ERK1 induces epithelial-to-mesenchymal transformation via DEF motif-dependent signaling events. *Mol Cell* 38, 114–127, doi:10.1016/j.molcel.2010.02.020 (2010). [PubMed: 20385094]
16. Shin S et al. ERK2 regulates epithelial-to-mesenchymal plasticity through DOCK10-dependent Rac1/FoxO1 activation. *Proc Natl Acad Sci U S A* 116, 2967–2976, doi:10.1073/pnas.1811923116 (2019). [PubMed: 30728292]
17. Vashi P, Edwin P, Popiel B, Lammersfeld C & Gupta D Methylmalonic Acid and Homocysteine as Indicators of Vitamin B-12 Deficiency in Cancer. *PLoS One* 11, e0147843, doi:10.1371/journal.pone.0147843 (2016). [PubMed: 26807790]
18. Minn AJ et al. Genes that mediate breast cancer metastasis to lung. *Nature* 436, 518–524, doi:10.1038/nature03799 (2005). [PubMed: 16049480]
19. Miller FR, Miller BE & Heppner GH Characterization of metastatic heterogeneity among subpopulations of a single mouse mammary tumor: heterogeneity in phenotypic stability. *Invasion Metastasis* 3, 22–31 (1983). [PubMed: 6677618]
20. Broekaert D & Fendt SM Measuring In Vivo Tissue Metabolism Using (13)C Glucose Infusions in Mice. *Methods Mol Biol* 1862, 67–82, doi:10.1007/978-1-4939-8769-6_5 (2019). [PubMed: 30315460]
21. Yuan M, Breitkopf SB, Yang X & Asara JM A positive/negative ion-switching, targeted mass spectrometry-based metabolomics platform for bodily fluids, cells, and fresh and fixed tissue. *Nat Protoc* 7, 872–881, doi:10.1038/nprot.2012.024 (2012). [PubMed: 22498707]
22. Huttlin EL et al. The BioPlex Network: A Systematic Exploration of the Human Interactome. *Cell* 162, 425–440, doi:10.1016/j.cell.2015.06.043 (2015). [PubMed: 26186194]
23. Bos PD et al. Genes that mediate breast cancer metastasis to the brain. *Nature* 459, 1005–1009, doi:10.1038/nature08021 (2009). [PubMed: 19421193]
24. Mootha VK et al. PGC-1 α -responsive genes involved in oxidative phosphorylation are coordinately downregulated in human diabetes. *Nat Genet* 34, 267–273, doi:10.1038/ng1180 (2003). [PubMed: 12808457]
25. Subramanian A et al. Gene set enrichment analysis: a knowledge-based approach for interpreting genome-wide expression profiles. *Proc Natl Acad Sci U S A* 102, 15545–15550, doi:10.1073/pnas.0506580102 (2005). [PubMed: 16199517]
26. Oskarsson T et al. Breast cancer cells produce tenascin C as a metastatic niche component to colonize the lungs. *Nat Med* 17, 867–874, doi:10.1038/nm.2379 (2011). [PubMed: 21706029]

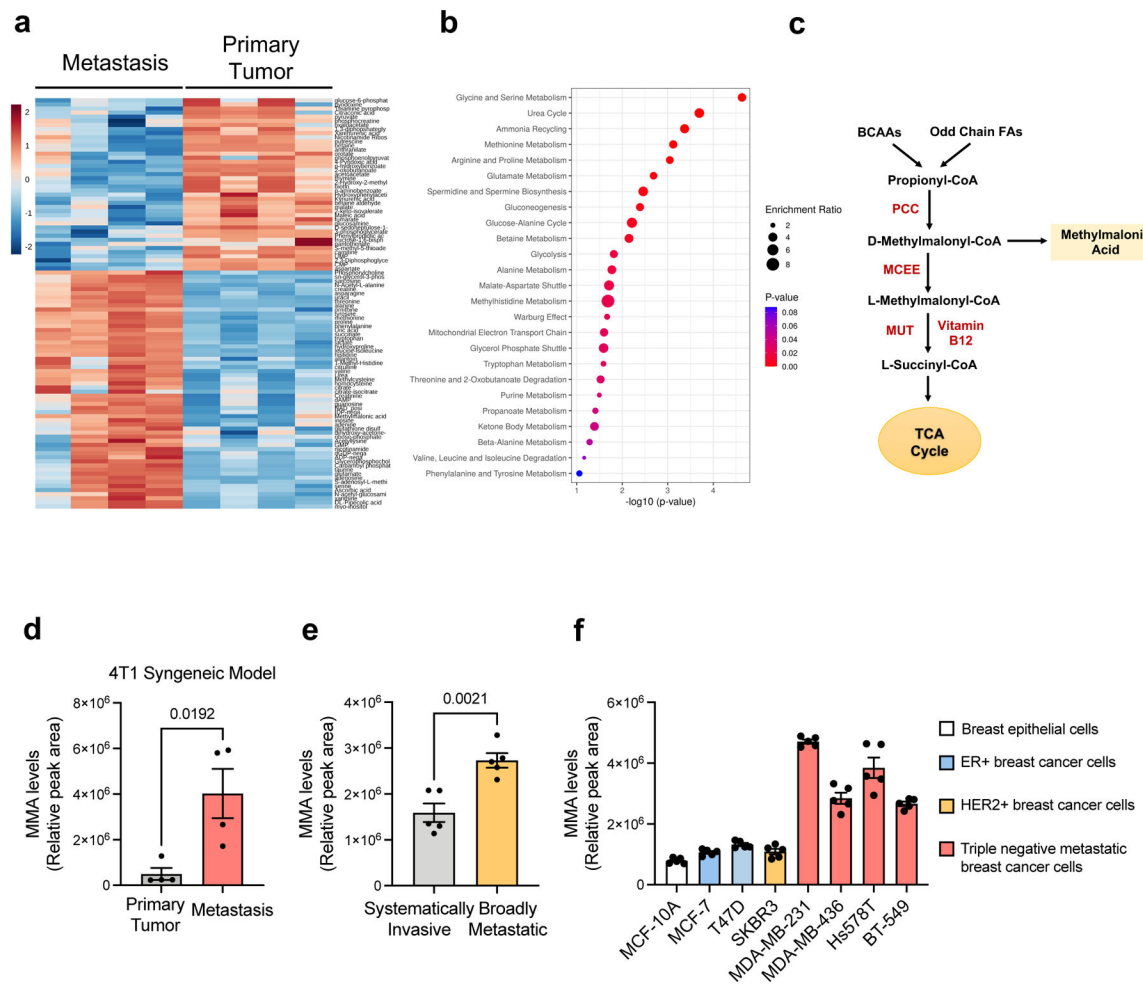


Fig. 1: Methymalonic Acid is upregulated in breast cancer metastasis.

a, b, Heat map (**a**) and metabolic pathway enrichment analysis (**b**) of the statistically significantly altered metabolites (FDR 0.05) in 4T1 primary tumors and pulmonary metastases (n=4 biologically independent samples). **c**, Schematic representation of propionate metabolism. **d**, Methymalonic acid (MMA) levels in 4T1 primary tumors and pulmonary metastases (n=4, two-tailed *t*-test). **e**, MMA levels in 4T1 (broadly metastatic) and 4T07 (locally invasive) clones with different metastatic potential derived from a single primary tumor (n=5 biologically independent samples, two-tailed *t*-test). **f**, MMA levels in breast epithelial and breast cancer cell lines (n=5 biologically independent samples). All values are expressed as mean \pm SEM.

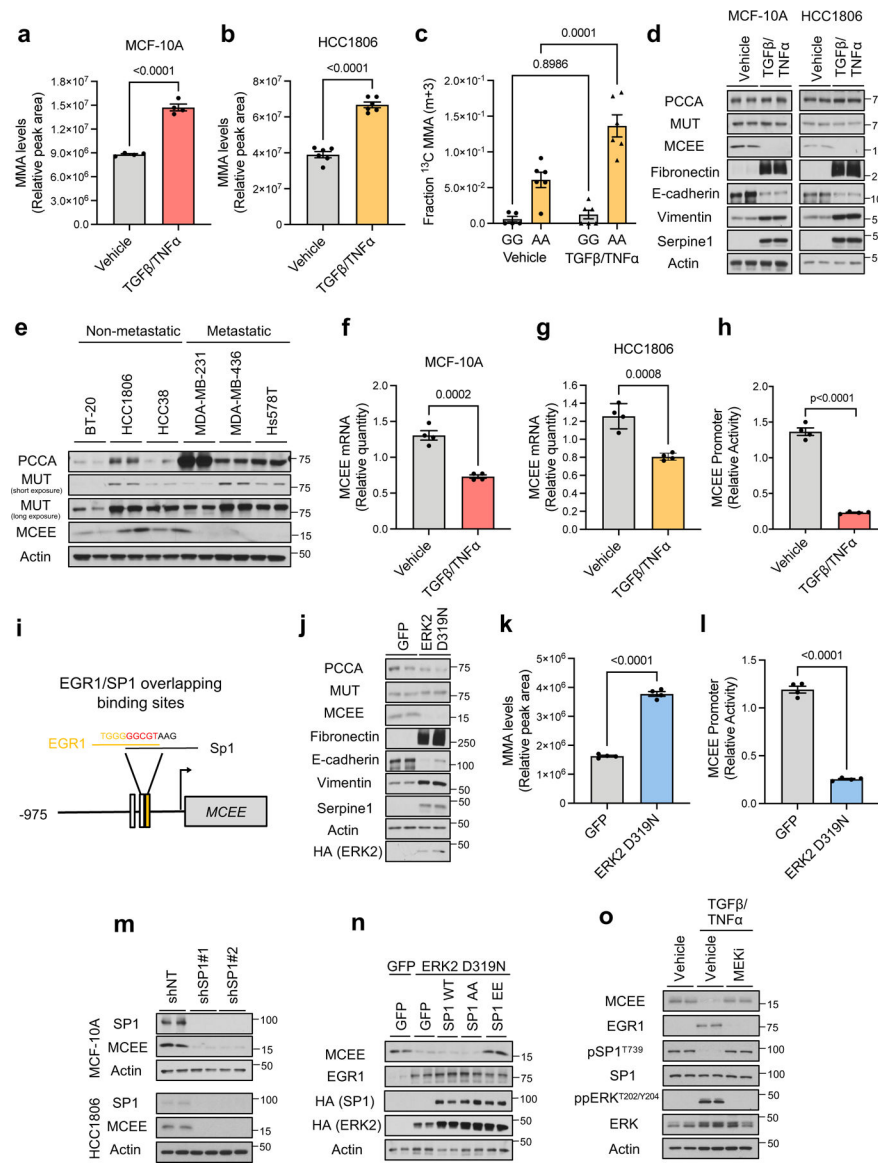


Fig. 2: Metastatic signaling leads to MMA production through regulation of MCEE.
a, b, MMA levels in MCF-10A (**a**) and HCC1806 (**b**) cells treated with TGFβ + TNFα for 3 days (n=4 biologically independent samples, two-tailed *t*-test). **c**, Fractions of labeled intracellular MMA derived from glucose + glutamine (GG) or valine + isoleucine + threonine + methionine (AA) in HCC1806 cells treated with TGFβ + TNFα for 3 days (n=6 biologically independent samples, two-way ANOVA with Sidak's multiple comparison test). **d, e**, Propionate metabolism-related enzyme levels evaluated by immunoblots in MCF-10A and HCC1806 cells treated with TGFβ + TNFα for 3 days (**d**), and in non-metastatic and metastatic triple negative breast cancer human cell lines (**e**); representative images (n=4 biologically independent samples). **f, g**, MCEE mRNA levels evaluated by qPCR in MCF-10A (**f**) and HCC1806 (**g**) cells treated with TGFβ + TNFα for 3 days (n=4 biologically independent samples, two-tailed *t*-test). **h**, MCEE-luciferase promoter activity in MCF-10A cells treated with TGFβ + TNFα for 3 days (n=4 biologically independent

samples, two-tailed *t*-test). **i**, Schematic representation of SP1 and EGR1 binding sites in MCEE promoter. **j**, Propionate metabolism-related enzyme levels evaluated by immunoblots in MCF-10A cells expressing the metastatic-inducer ERK2 D319N mutant for 3 days; representative images (n=4 biologically independent samples). **k**, MMA levels in MCF-10A cells expressing the metastatic-inducer ERK2 D319N mutant for 3 days (n=4 biologically independent samples, two-tailed *t*-test). **l**, MCEE-luciferase promoter activity in MCF-10A cells expressing the metastatic-inducer ERK2 D319N mutant for 3 days (n=4 biologically independent samples, two-tailed *t*-test). **m, n**, MCEE protein levels evaluated by immunoblot in MCF-10A and HCC1806 cells with SP1 knockdown for 3 days (**m**) and in MCF-10A cells expressing the ERK2 D319N mutant and either SP1 wild-type or the SP1 T453/T739 phosphorylation site mutants (S to A phospho-defective mutant; S to E, phospho-mimetic mutant) for 3 days (**n**); representative images (n=4 biologically independent samples). **o**, MCEE, EGR1 and phospho SP1 protein levels evaluated by immunoblot in HCC1806 treated with TGFβ + TNFα or TGFβ + TNFα + MEK inhibitor for 3 days; representative images (n=4 biologically independent samples). All values are expressed as mean ± SEM.

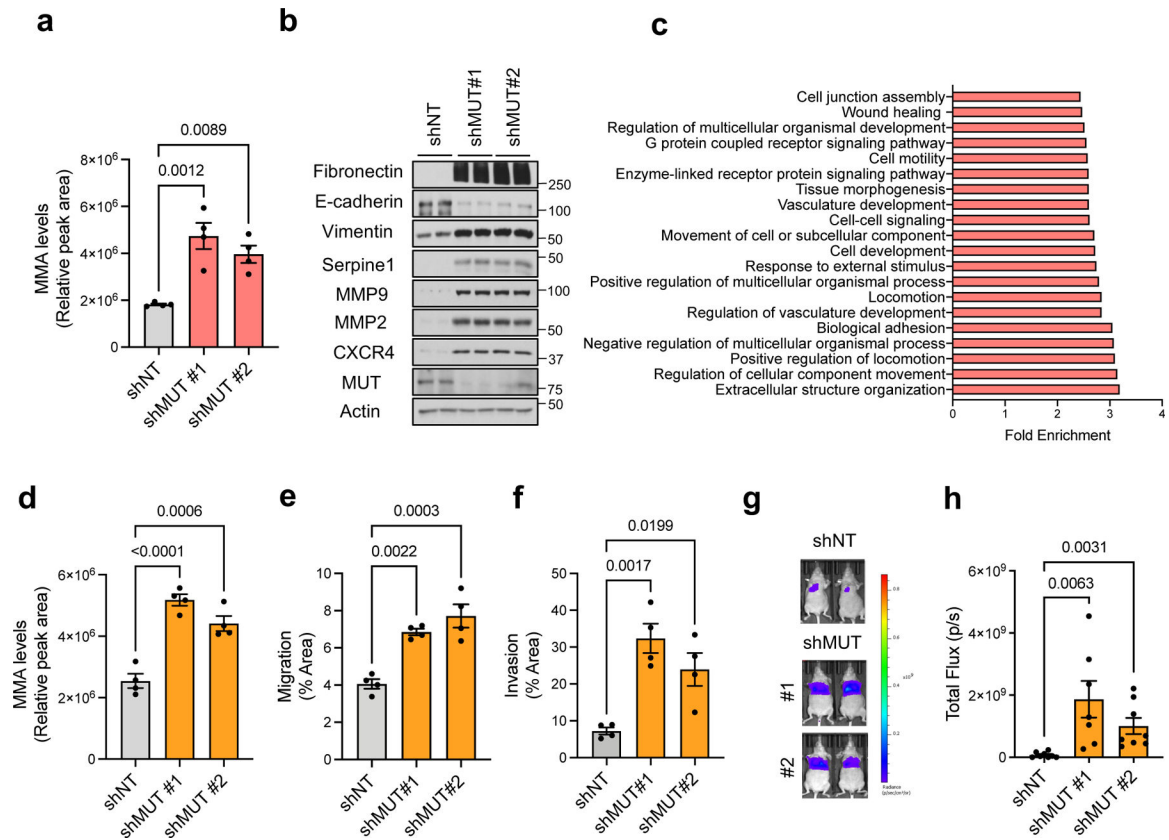


Fig. 3: Intracellular MMA production promotes EMT and aggressive properties.

a, b, MMA levels (one-way ANOVA with Tukey's multiple comparison test) (**a**) and immunoblots for EMT and aggressiveness markers (**b**) in HCC1806 cells with MUT knockdown for 3 days; representative images (n=4 biologically independent samples). **c**, Functional annotation clustering analysis of mRNAs that changed >1.5-fold when evaluated by RNA sequencing in A549 cells with MUT knockdown for 3 days (n=3 biologically independent samples). **d**, MMA levels in MDA-MB-231-luciferase parental cells with MUT knockdown for 3 days (n=4 biologically independent samples, one-way ANOVA with Tukey's multiple comparison test). **e, f**, Transwell migration (**e**) or invasion (**f**) assays of MDA-MB-231-luciferase parental cells with knockdown of MUT for 6 days (n=4 biologically independent samples, one-way ANOVA with Tukey's multiple comparison test). **g, h**, Lung colonization assay of MDA-MB-231-luciferase parental cells injected after 6 days of MUT knockdown imaged at 6 weeks; representative images (**g**) and quantification (**h**) (n=8 biologically independent animals for shNT and shMUT#2 and n=7 for shMUT#1, one-way ANOVA with Tukey's multiple comparison test). All values are expressed as mean ± SEM.

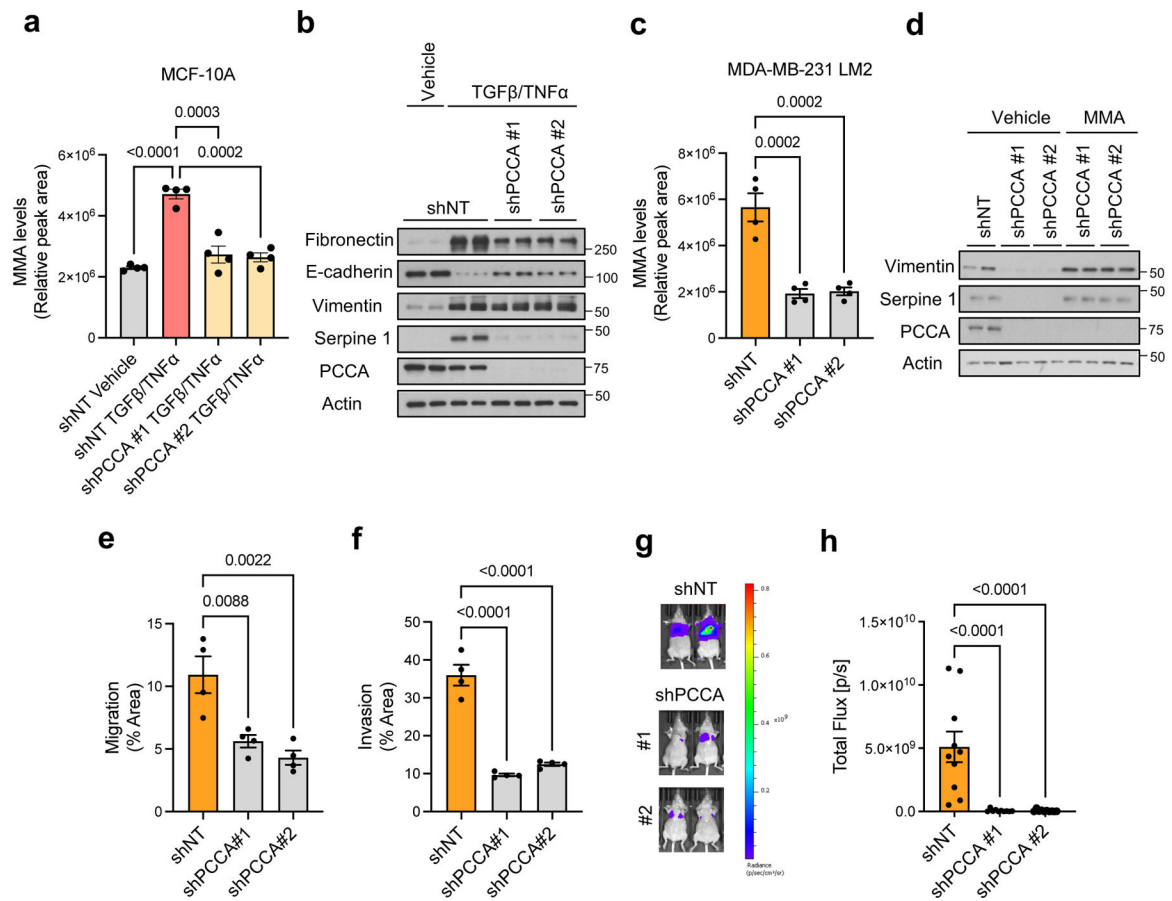


Fig. 4: PCC regulates MMA levels and determines pro-aggressive properties.

a, MMA levels in MCF-10A cells with PCCA knockdown and treated with TGFβ + TNFα for 3 days (n=4 biologically independent samples, two-way ANOVA with Sidak's multiple comparison test). **b**, EMT-related proteins evaluated by immunoblots in MCF-10A cells with PCCA knockdown and treated with TGFβ + TNFα for 5 days; representative images (n=4 biologically independent samples). **c**, MMA levels in MDA-MB-231-LM2 cells with PCCA knockdown for 5 days (n=4 biologically independent samples, one-way ANOVA with Tukey's multiple comparison test). **d**, Mesenchymal protein levels evaluated by immunoblots in MDA-MB-231-LM2 cells with PCCA knockdown and treated with 5 mM MMA for 5 days; representative images (n=4 biologically independent samples). **e**, **f**, Transwell migration (**e**) or invasion (**f**) assays of MDA-MB-231-luciferase LM2 cells with knockdown of PCCA for 6 days (n=4 biologically independent samples, one-way ANOVA with Tukey's multiple comparison test). **g**, **h**, Lung colonization assay of MDA-MB-231-luciferase LM2 cells with knockdown of PCCA for 6 days; representative images (**g**) and quantification (**h**) (n=10 biologically independent animals, one-way ANOVA with Tukey's multiple comparison test). All values are expressed as mean ± SEM.

Table.

Human Primers Used for qPCR Analysis, Related to Experimental Procedures

Gene		Primer Sequence
<i>TBP</i>	Forward	GAGCCAAGAGTGAAGAACAGTC
	Reverse	GCTCCCCACCATATTCTGAATCT
<i>ACTB</i>	Forward	CATGTACGTTGCTATCCAGGC
	Reverse	CTCCTTAATGTCACGCACGAT
<i>MCEE</i>	Forward	TTCATCCATTGGGACGTGAC
	Reverse	CTCTTCACTTAGACTGCCGGATC

Author Manuscript

Author Manuscript

Author Manuscript

Author Manuscript